Available online at www.sciencedirect.com
SCIENCE DIRECT®
Biochemical and Biophysical Research Communications 324 (2004) 489–496
BBRC
www.elsevier.com/locate/ybbrc

Modulation of repulsive forces between neurofilaments by sidearm phosphorylation

Sanjay Kumar[a,1], Jan H. Hoh[a,b,*]

[a] Department of Physiology, Johns Hopkins University School of Medicine, Baltimore, MD 21205, United States
[b] Department of Chemical Engineering, Johns Hopkins University, Baltimore, MD 21218, United States

Received 2 September 2004
Available online 28 September 2004

Abstract

Recent studies have advanced the notion that the axonal organization of neurofilaments (NFs) is based on mutual steric repulsion between the unstructured "sidearm" domains of adjacent NFs. Here, we present experimental evidence that these repulsive forces are modulated by the degree of sidearm phosphorylation. When NFs are sedimented into a gelatinous pellet, pellet volume falls with increasing ionic strength and enzymatic dephosphorylation; sedimentation of phosphorylated NFs in the presence of divalent cations also dramatically reduces pellet volume. Further, atomic force microscopy imaging of isolated mammalian NFs reveals robust exclusion of colloidal particles from the NF backbone that is reduced at high ionic strength and attenuated when the filaments are enzymatically dephosphorylated. Phosphate–phosphate repulsion on the NF sidearm appears to modulate NF excluded volume in a graded fashion, thereby controlling axonal NF organization through interfilament forces.

Keywords: Cytoskeleton; Intermediate filaments; Atomic force microscopy; Polymer brush; Polyelectrolyte; Cell mechanics; Unstructured proteins; Protein gels; Calcium; Phosphorylation; Amyotrophic lateral sclerosis

Neurofilaments (NFs) are an abundant and important cytoskeletal element of large, myelinated neurons. Vertebrate NFs are composed of three polypeptide subunits: a light chain (NF-L, 61 kDa in humans), a medium chain (NF-M, 90 kDa), and a heavy chain (NF-H, 110 kDa). The amino termini of the monomers contain rod domains which associate to form the filament backbone, and the carboxy termini of NF-M and -H form "sidearms" that protrude from the filament backbone [1–4]. Cross-sections of motor neurons show that NFs have a unique organization; they nonrandomly fill the bore of the axon with a characteristic interfilament spacing of 35–40 nm. Further, NF–NF spacing appears to be modulated by phosphorylation. and the level of phosphorylation has been correlated with NF–NF spacing in vivo in many axonal settings [5–8]. This modulation is graded in the sense that interfilament spacing appears to depend on phosphorylation in a relatively smooth fashion. However, our understanding of the molecular mechanism through which phosphorylation controls spacing remains incomplete.

A number of models have been advanced to explain the organization of neurofilaments and the relatively large interfilament distances. Perhaps the most prominent of these is the cross-bridge model, where the sidearms of neighboring NFs noncovalently bind one another [9–11]. A model based on direct electrostatic repulsion between the phosphorylated sidearms of neighboring filaments has also been proposed, although it has garnered less attention than the cross-bridge

* Corresponding author. Fax: +1 410 614 3797.
E-mail address: jhoh@jhmi.edu (J.H. Hoh).
[1] Present address: Vascular Biology Program, Children's Hospital Boston, Harvard Medical School Boston, MA 02115, USA.

0006-291X/$ - see front matter © 2004 Elsevier Inc. All rights reserved.
doi:10.1016/j.bbrc.2004.09.076

model [5,12]. More recently, the sidearms have been proposed to be highly unstructured polypeptides that undergo rapid Brownian motion to occupy a large effective volume, producing an entropic repulsion when two NFs are brought near one another [13–16].

The entropic repulsion model allows one to invoke conceptual and analytical frameworks developed to describe non-biological polymers [17]. Because NF sidearms contain an abundance of both positively and negatively charged residues (155 anionic residues, 154 cationic residues in the case of human NF-H), they may be classified as polyampholyte chains [18,19]. Synthetic polyampholytes have been studied extensively on both a theoretical level [20–22] and an experimental level [23–25], and two important lessons emerge from this work. First, polyampholyte properties often depend strongly on ionic strength. Second, in cases where polyampholytes contain titratable groups (so-called annealed chains), changes in pH can substantially influence polyampholyte physical properties. Thus, by altering intramolecular electrostatic interactions, one may manipulate the structure of polyampholyte chains and therefore the properties of the structures into which they self-assemble, including gels.

NFs form viscoelastic gels under appropriate buffer conditions, and the properties of these gels offer insight into the interfilament interactions that drive gel assembly. Leterrier et al. [10] examined the gelation kinetics and viscoelastic properties of NF gels using cone-and-plate rheometry. They found that NF gels have very large elastic moduli compared to other intermediate filaments of comparable molecular weight (e.g., vimentin), a property which was ascribed to specific cross-bridging between the sidearms. Both the kinetics of gel formation and the equilibrium viscoelastic properties were found to depend on the presence of phosphoinositides and actin filaments. In a later report, a "switch" model was proposed to explain this regulation in which the sidearm of a NF either binds to its own backbone or to the sidearm of an adjacent NF depending on sidearm phosphorylation, the presence of various NF-associated proteins, and divalent cation concentration [26].

The hypothesis that NF organization is influenced by the polyampholyte nature of NF sidearms predicts that interfilament interaction forces should vary with sidearm phosphorylation and key electrostatic properties of the buffer: ionic strength, pH, and divalent cation concentration. Here, we examine those relationships and interpret our findings in terms of polyampholyte behavior. We reconstitute mammalian NFs into gels under different buffer conditions and assay for excluded volume by measuring the size of the pellet. We also perform atomic force microscopy (AFM) imaging on isolated NFs and correlate findings on the single-filament level to gel properties.

Materials and methods

Isolation of NFs from bovine spinal cord. NFs were isolated from bovine spinal cord (BSC) as described elsewhere [13,27]. BSC was obtained from a local slaughterhouse and held on ice until processing, which began within 45 min of resection from the animal. BSC was then diced into 1–2 cm slices and homogenized in buffer A (100 mM Mes, 1.0 mM EGTA, and 0.5 mM $MgCl_2$, pH 6.5) at 1.6 mL buffer per gram BSC. This mixture was then centrifuged at 34,500*g* at 4 °C for 30 min. The supernatant was decanted, made 30% glycerol by volume, mixed thoroughly, and incubated at 37 °C for 20 min. This resulting solution was then centrifuged at 158,000*g* for 2 h at 20 °C, yielding a pellet which is a concentrated, NF-rich gel. This gel was resuspended in the buffer of interest and used in experiments as described below. In some cases, the pellet was frozen in liquid nitrogen, stored at −80 °C, and thawed immediately prior to use, with no detectable change in properties after 2–3 months.

Preparation of NF pellets. For studies of NF gel volume, approximately 100 μL of pellet was resuspended in 1 mL Millipore-purified water (18 MΩ-cm) and split equally among a set of 1.5 mL Eppendorf tubes. Each tube was then centrifuged at 158,000*g* for 30 min at 20 °C using a tabletop microcentrifuge, the supernatant was discarded, and the resulting pellet was resuspended in the buffer of interest. Each tube was then centrifuged again and resuspended again. After 3–4 cycles of centrifugation and resuspension, the top margin of the pellet was marked and measured using a micrometer caliper. Each sedimentation was performed along with an internal standard containing the same total mass of NFs. Results are reported as the relative pellet size which is the ratio of the pellet height for a given sample to that of the standard.

AFM imaging of single NFs. For studies of isolated NFs, approximately 2–5 μL of pellet was resuspended in 1 mL of the buffer of interest. Fifty microliters of this suspension was adsorbed on freshly cleaved ruby red muscovite mica (grade V1 or V2, Asheville–Schoonmaker Mica, Newport News, VA) at room temperature for 15 s and washed with 5 mL buffer. The sample was then transferred to the AFM stage for imaging at room temperature. Images were obtained with a Multimode AFM with a Nanoscope III or IIIa controller (Digital Instruments, Santa Barbara, CA), using a glass fluid cell. Imaging was performed with Olympus silicon nitride cantilevers (OMCL-TR400PSA) with lengths of 200 μm and nominal spring constants of 0.02 N/m and with C-type silicon nitride "Microlever" cantilevers (Digital Instruments) with lengths of 320 μm and nominal spring constants of 0.01 N/m. Prior to imaging, the microscope, sample, and cantilever were allowed to equilibrate at room temperature for at least 1 h. All images were collected in contact mode.

Enzymatic treatment of NFs. The dephosphorylation protocol was based on previous reports [28,29]. First, 100 μL NF pellet was resuspended in water as described above. To this suspension was added 5 μL of bovine calf intestine alkaline phosphatase (106.95 U/μl, Sigma Chemical, St. Louis, MO). The reaction mixture was then incubated at 37 °C for 5 h. For gel studies, the resulting suspension was repeatedly centrifuged and resuspended in the buffer of interest as described above, thus removing enzyme via the supernatant in the process. For AFM imaging, 5 μL of the reaction mixture was diluted into the buffer of interest and adsorbed and imaged as described.

Results

When a suspension of NFs is centrifuged at sufficiently high speed, the NFs form a gelatinous pellet. As the pellet size increases, the effective volume occupied by each NF increases and the mean interfilament spacing increases. To examine the effects of buffer conditions

and NF biochemistry on NF–NF spacing, we performed an assay for pellet size (Fig. 1). In this assay, a suspension of NFs is evenly divided into several aliquots, and each aliquot is resuspended in a buffer of defined ionic strength, pH, and divalent cation (Ca^{2+} or Mg^{2+}) concentration. All aliquots are centrifuged together, yielding a set of pellets containing equal amounts of NFs. The relative volumes of the pellets therefore provide an indirect measure of interfilament spacing.

Because NF sidearms are polyampholytes, electrostatics are expected to play a significant role in determining sidearm structure and therefore NF–NF repulsion. As a result, NF–NF spacing should vary as a function of ionic strength. We examined this salt-dependence over a range of buffer pH values (Fig. 2). Similarly, the presence of multiple titratable groups on the NF sidearm (glutamine, lysine, and phosphoserine) predicts that the pH at which the experiment is conducted will strongly influence sidearm dimensions by altering charge. Over a wide pH range (4.4–9.2), pellet size decreases with increasing ionic strength. In the context of the steric repulsion model of NF organization, the corresponding decrease in NF–NF spacing with increasing salt concentration is due to condensation of NF sidearms. At all three pH values studied, most of this decrease occurs within a concentration range of 100–150 mM. Higher salt concentrations exert little additional influence on NF–NF spacing. The steepest ionic strength dependence is observed at pH 4.4, where the NF sidearm is expected to be strongly positively charged due to protonation of lysines in the KSP domains of NF-H. Here, changing the salt concentration from 10 to 110 mM reduces pellet size by 40%; conversely, at higher pH, comparable increases in salt concentrations produce more modest reductions in pellet size (approximately 25% at pH 6.8 and 20% at pH 9.2). As the pH is increased, the sidearms are expected to acquire a progressively negative charge as the glutamate and phosphoserine residues are deprotonated.

In addition to changes in ionic strength, electrostatic repulsive forces within the NF sidearm may be directly manipulated by reducing sidearm charge. By treating

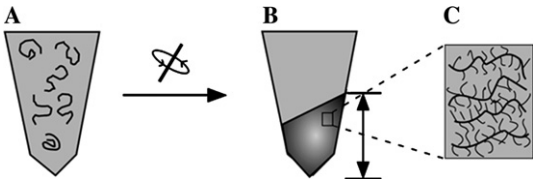

Fig. 1. Schematic of pellet size assay. NFs are resuspended in a buffer of given ionic strength, pH, and divalent cation concentration (A). The suspension is then gently sedimented, resulting in NF pellet formation (B). The resulting pellet height (arrows) is then normalized by the pellet height of an internal standard which contains the same total mass of NFs and is sedimented under identical conditions. The size of the pellet reflects mean interfilament spacing and the strength of interfilament repulsion (C). Note that in (A) the sidearms are omitted for clarity.

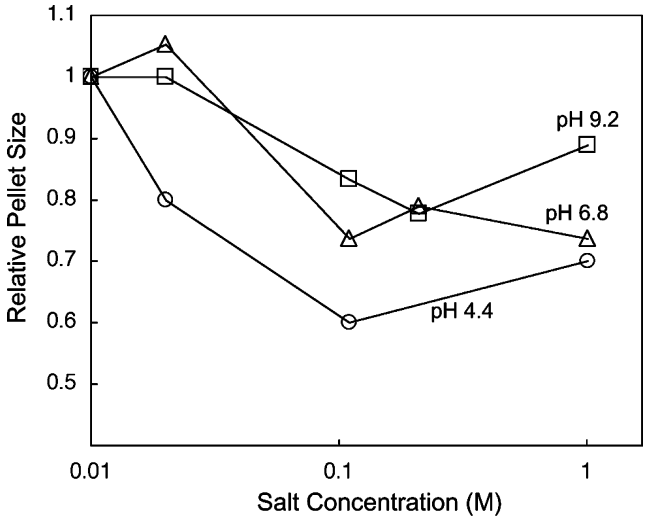

Fig. 2. Effect of salt concentration on NF pellet size. Relative pellet size is shown as a function of salt concentration at pH 4.4 (circles), pH 6.8 (triangles), and pH 9.2 (squares). The total salt concentration includes contributions from the MES buffer (10 mM in each case) and NaCl. In all cases, the error bars fall within the size of the marker ($n = 6$).

native NFs with alkaline phosphatase, phosphoserine residues are dephosphorylated (Fig. 3). Evidence for effective phosphorylation comes from gel electrophoresis, which demonstrates a predicted shift in molecular weight of NF-H and NF-M (inset) [28,29]. When dephosphorylated NFs are sedimented through a range of salt concentrations, pellet size varies only modestly. This is in contrast to native NFs, which show a steady reduction in pellet size with increasing salt concentra-

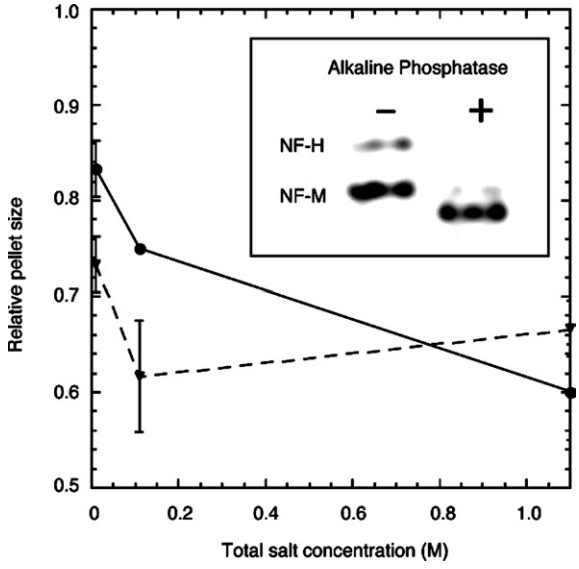

Fig. 3. Effect of phosphorylation state on NF pellet size. Relative pellet sizes are shown over a range of ionic strengths for native NFs (solid line) and NFs treated with alkaline phosphatase (dashed line). SDS–PAGE is used to assess the degree of phosphorylation (inset); the left and right lanes are control and enzyme-treated NFs, respectively. Each error bar represents the means ± one standard deviation ($n = 6$).

tion. The relatively shallow dependence of NF–NF spacing on salt concentration for dephosphorylated NFs is characteristic of behavior closer to the neutral chain limit, where repulsion between like-charged residues is balanced by electrostatic attraction between oppositely charged residues. The dramatic qualitative change in the salt-dependence of gel properties with dephosphorylation underscores the importance of phosphorylation to regulating NF–NF spacing.

The polyampholyte nature of NF sidearms may be further characterized by examining the effect of divalent cations on gel behavior. In addition to their obvious physiological significance, calcium and magnesium are known to strongly influence the viscoelastic properties of NF gels in vitro [28]. To probe this effect, we sedimented NFs in the presence of increasing concentrations of calcium and magnesium (Fig. 4). At a total concentration of only 5 mM, Mg^{2+} condenses NF pellets by approximately 22%. Increasing the concentration of Mg^{2+} by a factor of 10 produces only an additional 12% reduction in pellet size (Fig. 4A). Thus, small concentrations of Mg^{2+} significantly alter NF–NF spacing. These effects are reflected in the appearance of the pellets themselves (inset). Ca^{2+} produces a similar degree of condensation; addition of 5 mM Ca^{2+} produces a 28% reduction in pellet size (Fig. 4B).

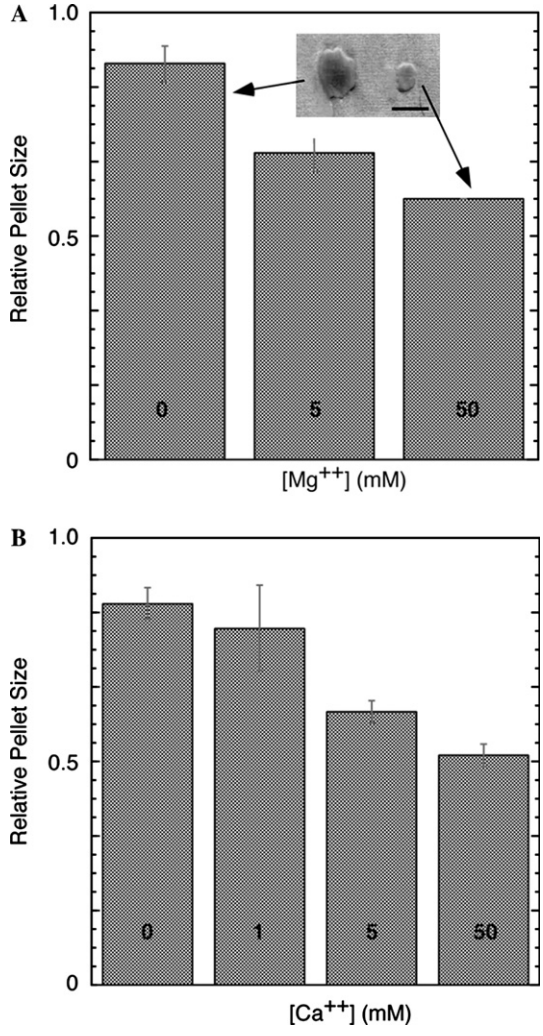

Fig. 4. Effect of divalent cation concentration. Relative pellet sizes in the presence of (A) Mg^{2+} and (B) Ca^{2+}. The inset in (A) depicts photographs of pellets obtained at 0 and 50 mM $MgCl_2$ (bar is 5 mm). All experiments were performed at 1 mM Mes, pH 6.8. Each error bar represents the means ± one standard deviation ($n = 6$).

To investigate the structural origins of the effect of phosphorylation on NF gel properties, we next used AFM to image single NFs. First, native NFs were adsorbed onto mica and imaged in buffer which included either 0 or 100 mM NaCl (Fig. 5). In these images, the NF backbones are clearly visible as snakelike filaments in a background of residual contaminants from the preparation. Surrounding each backbone is a zone of total width 100–150 nm from which these contaminants are excluded. The presence of these exclusion zones concurs with a previous report which attributed them to repulsive forces originating from the thermal motion of the unstructured sidearm domains [13]. Here, the exclusion zones are present at both relatively low and high salt concentrations, suggesting they do not originate from direct electrostatic repulsion between the NFs and the contaminants. When dephosphorylated NFs are examined under the same set of buffer conditions, we observe dramatically different results. As with native NFs, the backbones are again prominently visible. Now, however, the exclusion zones are dramatically diminished at 0 mM NaCl and essentially nonexistent at 100 mM NaCl.

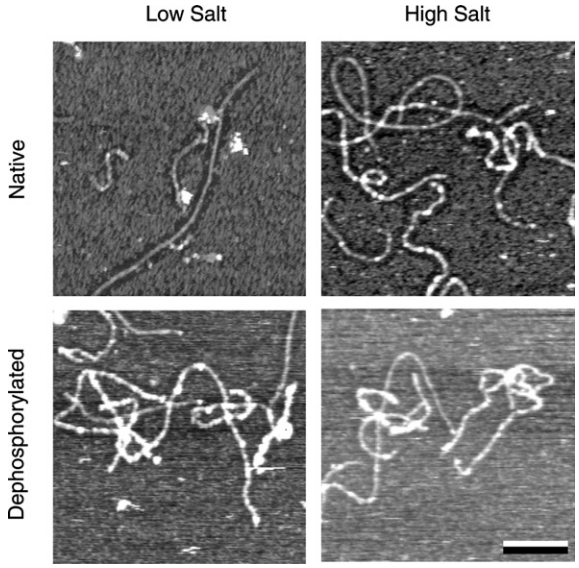

Fig. 5. AFM imaging of native and dephosphorylated neurofilaments. The top two panels depict native NFs, and the bottom two panels depict alkaline phosphatase-treated NFs. The images in the left column ("high salt") were obtained at 0 mM NaCl, and those in the right column ("low salt") were obtained at 100 mM NaCl. In addition to NaCl, each buffer contains 10 mM $MgCl_2$ and 10 mM Mes, pH 6.8. Scale bar is 500 nm.

Discussion

Several key findings emerge from our characterization of NF gels. In particular, gel volume falls with increasing ionic strength, reduced sidearm phosphorylation, and millimolar concentrations of calcium or magnesium. The size of the gelatinous NF pellet reflects the effective volume occupied by each NF and therefore serves as an indirect measure of mean NF–NF spacing and interaction force. In terms of the entropic repulsion model of NF–NF spacing, this reduced interaction force originates from condensation of sidearm domains. Condensation or collapse of charged polymers with increases in ionic strength is characteristic of behavior in the polyelectrolyte limit and occurs because the added salt screens repulsive forces between charged monomers [30]. This notion has been validated on several levels, including the radius of gyration of single chains [31], the diameter of coated spherical particles [32], and the thickness and interaction forces of adsorbed polymer layers [24]. This is in contrast to behavior in the neutral chain limit, where polymer chain volume may rise with increased ionic strength [33]. The most obvious origin of chain charge in the NF sidearm is the abundance of phosphoserine residues in NF-H. In this model, electrostatic repulsion between negatively charged residues (phosphoserines, aspartates, and glutamates) within the sidearm determines the thickness of the sidearm layer over a wide range of pH and that these repulsive forces are screened with added salt.

Further support for phosphorylation as an important regulator of NF–NF spacing comes from experiments in which the sidearms are enzymatically dephosphorylated (Fig. 3). The pellet size of dephosphorylated NFs is smaller than that of native NFs and depends much less steeply on ionic strength. This type of ionic strength-dependence is more characteristic of neutral chain behavior, where both attractive and repulsive forces within the polypeptide chain are important determinants of chain volume. This agrees well with the behavior expected from the composition of unmodified mammalian NF-H sequences, which contain closely balanced numbers of anionic and cationic residues. In vitro, enzymatic dephosphorylation produces dramatic changes in both the gelation kinetics and viscoelastic properties of NF gels [28]. In addition, thin section electron microscopy of fixed and stained NFs has shown that dephosphorylated NFs are considerably more densely packed than native NFs [29].

The finding that NF pellets are condensed by divalent cations provides further evidence for the structural importance of phosphorylation. In synthetic polymer systems, divalent cations have been shown to produce short-ranged attractive forces, leading to attraction between normally repulsive polymer-coated surfaces [34]. In the case of NFs, $MgCl_2$ produces profound increases in NF viscosity [35], and $AlCl_3$ induces NF aggregation in vitro [27]. In the context of the entropic repulsion model, multivalent cations would serve to attenuate NF–NF repulsion by condensing the sidearms. At sufficiently large concentrations, multivalent cations would convert the normally repulsive NF–NF interaction into an attractive one, leading to NF aggregation in the pathological case. Indeed, NF sidearms have been postulated to serve as a buffer for divalent cations in healthy neurons; in neurodegenerative pathologies such as ALS, it has been proposed that large increases in intracellular calcium overwhelm the buffer system, leading to NF aggregation and ultimately cell death [36].

The AFM experiments provide direct structural support for this model of the role of phosphorylation. Native, phosphorylated NFs produce robust exclusion of contaminants even at high (>100 mM) monovalent salt concentrations, a signature of polymer brush-like behavior [13]. When dephosphorylated, these exclusion zones are greatly attenuated at low salt concentration and essentially ablated at high salt concentration, implying that the sidearms occupy a smaller effective volume. It is interesting to note that individual sidearms are never distinctly visible in any of the images presented here, even in the complete absence of exclusion zones. One reason for this is the limited lateral resolution of the AFM tip coupled with the relatively high density of NFs along the backbone; EM of single NFs show that sidearms are spaced 2–5 nm apart along the backbone, a distance far smaller than the dimensions of a typical AFM tip [1]. Second, when they condense in response to changes in phosphorylation or buffer conditions, the sidearms may collapse onto the backbone. In fact, Gou et al. [26] propose a model in which inter- and intrafilament interactions act reciprocally to modulate the structure and mechanical properties of NF gels.

The notion that phosphorylation controls NF organization through intramolecular repulsive forces offers insight into the control of NF architecture in the axon; in particular, it suggests that phosphorylation acts as a graded switch that modulates the structure of the entire cytoskeleton through changes in relatively short-range repulsive interactions. In vivo, phosphorylation levels are determined by a balance between the activities of intracellular kinases and phosphatases which regulate the degree of sidearm phosphorylation (Fig. 6). Importantly, activation of many of these enzymes are events in signal transduction cascades, including signaling through growth and stress factor receptors, integrins, and calcium channels [37]. Phosphorylation-dependent NF remodeling may therefore represent a key endpoint in the conversion of extracellular biochemical cues into changes in axonal size and mechanics.

While many lines of evidence support NF phosphorylation as an important determinant of NF–NF spacing in vivo, the relative importance of NF-M and NF-H phosphorylation remains controversial. Recently,

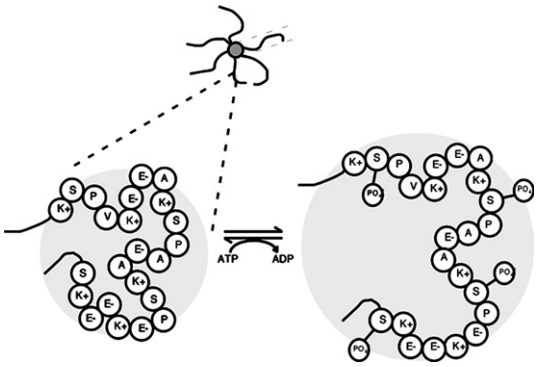

Fig. 6. Schematic of phosphorylation-based control of sidearm conformation. The upper diagram is a NF viewed in cross-section, with the sidearms emerging from the backbone. The native NF sidearm sequence is composed of KSP repeats which contain an abundance of charged residues which nearly balance one another in number. When the sidearm is enzymatically phosphorylated, the sidearm acquires a strong net negative charge causing the chain to expand as a consequence of osmotic swelling and electrostatic repulsion, producing greater NF–NF spacing.

transgenic mice have been developed that express truncated NF-H and/or NF-M subunits without tail phosphorylation sites [38–40]. Mice expressing truncated NF-M subunits exhibit reduced axonal caliber, axonal radial growth, and interfilament spacing in the setting of either wild-type or truncated NF-H. Surprisingly, however, while mice in which only NF-H is truncated do exhibit retarded axonal radial growth, axonal caliber and interfilament spacing in vivo are similar to wild-type [39]. It is important to emphasize that these findings do not preclude an entropic repulsion model based on graded NF phosphorylation. First, NF-M itself has several phosphorylation sites (e.g., human NF-M contains 10 KSP repeats); assuming a pK_a for double ionization of 6.3 [41], complete phosphorylation at physiologic pH would add a negative charge of 20. Indeed, NF-M phosphorylation is elevated in NF-H null mice, suggesting a compensatory mechanism [42]. Second, mice lacking NF-H tails exhibit some subtle but critical cytoskeletal phenotypic properties; most importantly, when viewed in quick-freeze deep-etch preparations, NFs in these mice come into frequent lateral apposition [39]. These intimate lateral contacts are rarely observed in wild-type axons, consistent with a picture in which the highly phosphorylated NF-H serves as a spacing element that opposes longitudinal NF aggregation. Thus, even if NF-M is the key modulator of axonal NF organization, both NF-M and NF-H phosphorylation appear to be important in shaping the details of that organization. Indeed, a model in which NF-M establishes a baseline NF excluded volume and in which NF-H phosphorylation "fine-tunes" this volume and offers graded control of NF–NF spacing would reconcile the transgenic mouse studies described above and the biochemical studies reported here.

Given a model in which NF organization is determined by predominantly repulsive forces, it is curious that NFs form compact gels at all. However, it is important to remember that the formation of these gels is greatly facilitated by centrifugation. Indeed, when a pellet is mechanically disrupted, NFs disperse back into solution. Similarly, when the axonal membrane is chemically disrupted, axonal NFs are observed to diffuse apart [43]. Presumably, then, sedimentation forces overcome NF–NF repulsion and allow effective attractive forces to play a significant structural role. These attractive forces may originate from entanglement or higher-order self-assembly of whole NF backbones. Support for such structures comes from studies with neuroblastoma cells in culture, which reveal that individual and bundled NFs coexist in growing neurites [44]. NF entanglement and self-assembly would also be facilitated by regional variations in sidearm phosphorylation along the NF backbone. Such diversity would not be unexpected, given that sidearm phosphates are markedly heterogeneous in their susceptibility to enzymatic cleavage [28]. Such variations would produce substantial regional differences in sidearm charge, excluded volume, and repulsive forces.

Two recent reports have addressed the role of phosphorylation in controlling sidearm conformations in vitro and in modulating interactions between NFs and mitochondria in vivo. Aranda-Espinoza et al. [45] found that dephosphorylated NF sidearms occupy a smaller effective volume than phosphorylated sidearms, as measured by light scattering and AFM-based force spectroscopy. Surprisingly, however, less force was needed to fully extend dephosphorylated sidearms than phosphorylated sidearms, suggesting the presence of intramolecular *attractive* forces mediated by phosphates. Specifically, the authors hypothesized that electrostatic "bridging" between phosphoserines and lysines in the KSP repeats is an important determinant of sidearm conformation. The second report [46] provided evidence that sidearm phosphorylation modulates binding between NFs and mitochondria in a manner that depends on the mitochondrial potential. The finding that NF–NF forces appear attractive in some experimental contexts and repulsive in others reinforces an emerging consensus that NFs in vivo are highly heterogeneous, with widely varying degrees of phosphorylation and propensity to assemble into higher-order structures. Clearly, elucidating the physicochemical details of this complex equilibrium and its consequences in vivo represents a substantial and ongoing challenge to understanding NF physiology.

There are several important limitations to the gel volume measurements presented here. First, the results of the assay are not directly interpretable in terms of NF–NF spacing distances; instead, trends in these distances are inferred through changes in gel volume.

Second, the assay does not precisely measure the specific volume (i.e., volume per NF). This results from the geometry in which the assay is performed (pellet height along the vessel wall is used as a marker for volume), and the polydispersity of the filaments themselves. However, the relative pellet sizes are likely underestimates of actual differences in gel volume. For example, when NF gels are treated with 50 mM $MgCl_2$ (Fig. 3A), gel size is reduced approximately 35% by the pellet height assay; however, inspection of the actual pellets (Fig. 3A, inset) suggests that the reduction in pellet size is considerably greater. This results from our using a single linear dimension to track differences in volume. For example, if the pellet is approximated as an ellipsoid, a 2-fold difference in each of two axial dimensions will produce a 4-fold difference in volume. Thus, the assay clearly yields a gross underestimate of differences in excluded volume, and efforts to develop more precise assays are warranted.

We have examined the properties of single NFs and NF gels as a function of sidearm phosphorylation and buffer conditions. In particular, we have shown that the volume of native NF gels decreases with increasing ionic strength over a wide pH range. When NFs are enzymatically dephosphorylated, this dependence becomes less steep. Native NF gel size also decreases in the presence of divalent cations at millimolar concentrations. AFM imaging of isolated NFs reveals that native NFs produce robust molecular exclusion even at high ionic strength, a property which is markedly attenuated when the sidearms are dephosphorylated. Taken together, these results suggest that the native NF sidearm acts functionally like a polyampholyte in vivo whose conformational properties are determined by the level of phosphorylation and the concentration of divalent cations. At high phosphorylation levels, the sidearm lies in the polyelectrolyte limit; as the sidearm is dephosphorylated, conformational behavior approaches the neutral chain limit. In the context of the entropic repulsion model, the degree of sidearm phosphorylation modulates the volume occupied by the NF sidearm through intramolecular electrostatic repulsion.

Acknowledgments

This work was supported by the National Institutes of Health (Medical Scientist Training Program Fellowship to S.K.) and the US Army (DAMD 17-99-1-9488 to J.H.H.).

References

[1] N. Geisler, K. Weber, Self-assembly in vitro of the 68,000 molecular-weight component of the mammalian neurofilament triplet proteins into intermediate-sized filaments, J. Mol. Biol. 151 (1981) 565–571.
[2] S. Hisanaga, N. Hirokawa, Structure of the peripheral domains of neurofilaments revealed by low-angle rotary shadowing, J. Mol. Biol. 202 (1988) 297–305.
[3] R.D. Leapman, P.E. Gallant, T.S. Reese, S.B. Andrews, Phosphorylation and subunit organization of axonal neurofilaments determined by scanning transmission electron microscopy, Proc. Natl. Acad. Sci. USA 94 (1997) 7820–7824.
[4] M. Willard, C. Simon, Antibody decoration of neurofilaments, J. Cell Biol. 89 (1981) 198–205.
[5] S.M. de Waegh, V.M.Y. Lee, S.T. Brady, Local modulation of neurofilament phosphorylation, axonal caliber, and slow axonal transport by myelinating schwann cells, Cell 68 (1992) 451–463.
[6] R. Martin, R. Door, A. Ziegler, W. Warchol, J. Hahn, D. Breitig, Neurofilament phosphorylation and axon diameter in the squid giant fibre system, Neuroscience 88 (1999) 327–336.
[7] M.J. Strong, W.L. Strong, H. Jaffe, B. Traggert, M.M. Sopper, H.C. Pant, Phosphorylation state of the native high-molecular-weight neurofilament subunit protein from cervical spinal cord in sporadic amyotrophic lateral sclerosis, J. Neurochem. 76 (2001) 1315–1325.
[8] X. Yin, T.O. Crawford, J.W. Griffin, P.H. Tu, V.M.Y. Lee, C.M. Li, J. Roder, B.D. Trapp, Myelin-associated glycoprotein is a myelin signal that modulates the caliber of myelinated axons, J. Neurosci. 18 (1998) 1953–1962.
[9] J.G. Chen, T. Nakata, Z.Z. Zhang, N. Hirokawa, The C-terminal tail domain of neurofilament protein-H (NF-H) forms the crossbridges and regulates neurofilament bundle formation, J. Cell Sci. 113 (2000) 3861–3869.
[10] J.F. Leterrier, J. Kas, J. Hartwig, R. Vegners, P.A. Janmey, Mechanical effects of neurofilament cross-bridges—modulation by phosphorylation, lipids, and interactions with F-actin, J. Biol. Chem. 271 (1996) 15687–15694.
[11] T. Nakagawa, J.G. Chen, Z.Z. Zhang, Y. Kanai, N. Hirokawa, Two distinct functions of the carboxyl-terminal tail domain of NF-M upon neurofilament assembly—cross-bridge formation and longitudinal elongation of filaments, J. Cell Biol. 129 (1995) 411–429.
[12] M.J. Carden, J.Q. Trojanowski, W.W. Schlaepfer, V.M.Y. Lee, Two-stage expression of neurofilament polypeptides during rat neurogenesis with early establishment of adult phosphorylation patterns, J. Neurosci. 7 (1987) 3489–3504.
[13] H.G. Brown, J.H. Hoh, Entropic exclusion by neurofilament sidearms: a mechanism for maintaining interfilament spacing, Biochemistry 36 (1997) 15035–15040.
[14] S. Kumar, X. Yin, B.D. Trapp, J.H. Hoh, M.E. Paulaitis, Relating interactions between neurofilaments to the structure of axonal neurofilament distributions through polymer brush models, Biophys. J. 82 (2002) 2360–2372.
[15] S. Kumar, X. Yin, B.D. Trapp, M.E. Paulaitis, J.H. Hoh, Role of long-range repulsive forces in organizing axonal neurofilament distributions: evidence from mice deficient in myelin-associated glycoprotein, J. Neurosci. Res. 68 (2002) 681–690.
[16] R. Mukhopadhyay, S. Kumar, J.H. Hoh, Molecular mechanisms for organizing the neuronal cytoskeleton, Bioessays 26 (2004) 1017–1025.
[17] J.N. Bright, T.B. Woolf, J.H. Hoh, Predicting properties of intrinsically unstructured proteins, Prog. Biophys. Mol. Biol. 76 (2001) 131–173.
[18] S.E. Kudaibergenov, Recent advances in the study of synthetic polyampholytes in solutions, Adv. Polymer Sci. 144 (1999) 115–197.
[19] M.N. Tamashiro, E. Hernandez-Zapata, P.A. Schorr, M. Balastre, M. Tirrell, P. Pincus, Salt dependence of compression normal forces of quenched polyelectrolyte brushes, J. Chem. Phys. 115 (2001) 1960–1969.

[20] A. Diehl, M.C. Barbosa, Y. Levin, Neutral polyampholyte in an ionic solution, Phys. Rev. E 54 (1996) 6516–6525.
[21] P.G. Higgs, J.F. Joanny, Theory of polyampholyte solutions, J. Chem. Phys. 94 (1991) 1543–1554.
[22] Y. Kantor, H. Li, M. Kardar, Conformations of polyampholytes, Phys. Rev. Lett. 69 (1992) 61–64.
[23] A.E. English, S. Mafe, J.A. Manzanares, X.H. Yu, A.Y. Grosberg, T. Tanaka, Equilibrium swelling properties of polyampholytic hydrogels, J. Chem. Phys. 104 (1996) 8713–8720.
[24] Y. Kamiyama, J. Israelachvili, Effect of pH and salt on the adsorption and interactions of an amphoteric polyelectrolyte, Macromolecules 25 (1992) 5081–5088.
[25] G. Nisato, J.P. Munch, S.J. Candau, Swelling, structure, and elasticity of polyampholyte hydrogels, Langmuir 15 (1999) 4236–4244.
[26] J.P. Gou, T. Gotow, P.A. Janmey, J.F. Leterrier, Regulation of neurofilament interactions in vitro by natural and synthetic polypeptides sharing Lys-Ser-Pro sequences with the heavy neurofilament subunit NF-H: neurofilament crossbridging by antiparallel sidearm overlapping, Med. Biol. Eng. Comput. 36 (1998) 371–387.
[27] J.C. Troncoso, J.L. March, M. Haner, U. Aebi, Effect of aluminum and other multivalent cations on neurofilaments in vitro—an electron-microscopic study, J. Struct. Biol. 103 (1990) 2–12.
[28] J. Eyer, J.F. Leterrier, Influence of the phosphorylation state of neurofilament proteins on the interactions between purified filaments in vitro, Biochem. J. 252 (1988) 655–660.
[29] T. Gotow, T. Tanaka, Y. Nakamura, M. Takeda, Dephosphorylation of the largest neurofilament subunit protein influences the structure of crossbridges in reassembled neurofilaments, J. Cell Sci. 107 (1994) 1949–1957.
[30] J.L. Barrat, J.F. Joanny, Theory of polyelectrolyte solutions, Adv. Chem. Phys. XCIV 94 (1996) 1–66.
[31] E. Fouissac, M. Milas, M. Rinaudo, R. Borsali, Influence of the ionic-strength on the dimensions of sodium hyaluronate, Macromolecules 25 (1992) 5613–5617.
[32] R. Hariharan, C. Biver, J. Mays, W.B. Russel, Ionic strength and curvature effects in flat and highly curved polyelectrolyte brushes, Macromolecules 31 (1998) 7506–7513.
[33] P. Cicuta, I. Hopkinson, Studies of a weak polyampholyte at the air-buffer interface: the effect of varying pH and ionic strength, J. Chem. Phys. 114 (2001) 8659–8670.
[34] T. Abraham, A. Kumpulainen, Z. Xu, M. Rutland, P.M. Claesson, J. Masliyah, Polyelectrolyte-mediated interaction between similarly charged surfaces: role of divalent counter ions in tuning surface forces, Langmuir 17 (2001) 8321–8327.
[35] J.F. Leterrier, J. Eyer, Properties of highly viscous gels formed by neurofilaments in vitro—a possible consequence of a specific interfilament cross-bridging, Biochem. J. 245 (1987) 93–101.
[36] L.P. Rowland, N.A. Shneider, Medical progress: amyotrophic lateral sclerosis, N. Engl. J. Med. 344 (2001) 1688–1700.
[37] P. Grant, H.C. Pant, Neurofilament protein synthesis and phosphorylation, J. Neurocytol. 29 (2000) 843–872.
[38] M.L. Garcia, C.S. Lobsiger, S.B. Shah, T.J. Deerinck, J. Crum, D. Young, C.M. Ward, T.O. Crawford, T. Gotow, Y. Uchiyama, M.H. Ellisman, N.A. Calcutt, D.W. Cleveland, NF-M is an essential target for the myelin-directed "outside-in" signaling cascade that mediates radial axonal growth, J. Cell Biol. 163 (2003) 1011–1020.
[39] M.V. Rao, J. Campbell, A.D. Yuan, A. Kumar, T. Gotow, Y. Uchiyama, R.A. Nixon, The neurofilament middle molecular mass subunit carboxyl-terminal tail domains is essential for the radial growth and cytoskeletal architecture of axons but not for regulating neurofilament transport rate, J. Cell Biol. 163 (2003) 1021–1031.
[40] M.V. Rao, M.L. Garcia, Y. Miyazaki, T. Gotow, A.D. Yuan, S. Mattina, C.M. Ward, N.A. Calcutt, Y. Uchiyama, R.A. Nixon, D.W. Cleveland, Gene replacement in mice reveals that the heavily phosphorylated tail of neurofilament heavy subunit does not affect axonal caliber or the transit of cargoes in slow axonal transport, J. Cell Biol. 158 (2002) 681–693.
[41] D.J. Graves, S.Q. Luo, Use of photoacoustic Fourier-transform infrared-spectroscopy to study phosphates in proteins, Biochem. Biophys. Res. Commun. 205 (1994) 618–624.
[42] M.V. Rao, M.K. Houseweart, T.L. Williamson, T.O. Crawford, J. Folmer, D.W. Cleveland, Neurofilament-dependent radial growth of motor axons and axonal organization of neurofilaments does not require the neurofilament heavy subunit (NF-H) or its phosphorylation, J. Cell Biol. 143 (1998) 171–181.
[43] A. Brown, R.J. Lasek, Neurofilaments move apart freely when released from the circumferential constraint of the axonal plasmamembrane, Cell Motil. Cytoskel. 26 (1993) 313–324.
[44] J.T. Yabe, T. Chylinski, F.S. Wang, A. Pimenta, S.D. Kattar, M.D. Linsley, W.K.H. Chan, T.B. Shea, Neurofilaments consist of distinct populations that can be distinguished by C-terminal phosphorylation, bundling, and axonal transport rate in growing axonal neurites, J. Neurosci. 21 (2001) 2195–2205.
[45] H. Aranda-Espinoza, P. Carl, J.F. Leterrier, P. Janmey, D.E. Discher, Domain unfolding in neurofilament sidearms: effects of phosphorylation and ATP, FEBS Lett. 531 (2002) 397–401.
[46] O.I. Wagner, J. Lifshitz, P.A. Janmey, M. Linden, T.K. McIntosh, J.F. Leterrier, Mechanisms of mitochondria-neurofilament interactions, J. Neurosci. 23 (2003) 9046–9058.